

POTENTIAL OF CONSUMER-GRADE CAMERAS AND PHOTOGRAMMETRIC GUIDELINES FOR SUBSURFACE UTILITY MAPPING

R. Z. M. Yuen¹, J. Boehm²

¹ SLA, Singapore Land Authority, 55 Newton Road, Revenue House #12-01, Singapore 307987 – royuyenzemin@gmail.com

² Dept. of Civil, Environmental & Geomatic Engineering, University College London, Gower Street, London, WC1E 6BT UK - j.boehm@ucl.ac.uk

Technical Commission II

KEY WORDS: Consumer-grade cameras, Smartphones, Digital cameras, SfM photogrammetry, Subsurface utilities, Underground mapping, Photogrammetric guidelines.

ABSTRACT:

The poor documentation of subsurface utility data is a common problem in many cities, exposing field engineers to risks of utility strike. This paper investigates the use of consumer-grade cameras to improve operational efficiency on construction sites and explores different imaging networks to optimize photogrammetric processing for low-cost subsurface utility surveys. Results from the first part of the study demonstrated the potential of consumer-grade cameras as a photogrammetric utility data acquisition tool. However, statistical insights from the photogrammetric calibration show that caution needs to be taken about the camera types particularly for lens calibration. Results from the second part of the study were recommended as easy-to-understand guidelines for image acquisition at trenches and supported the planning of photogrammetric measurements in the field.

1. INTRODUCTION

Driven by the increasing complexity of urban spaces and rapid infrastructure developments above and underground, city planners and engineers rely heavily on the knowledge and locations of subsurface utilities (electricity, gas, telecommunications, water, and drainage networks) for managing civil engineering projects. These services are crucial to the everyday life of citizens, providing communication, delivering gas, and supplying drinking water. Yet, the lack of reliable and accurate documentation of subsurface utility information (3D positional inaccuracies, missing, outdated and incomplete information of as-built utilities) (Hansen et al., 2020) affects not only citizens but different actors involved in the planning, construction, and management of buried assets.

The poor documentation of utility data exposes field engineers to health and safety risks associated with striking underground utilities (Al-Bayati and Panzer, 2019) due to insufficient information about the location, shape, twists and turns of cables and pipes. Utility strikes often result in wider disruptions, such as project overrun (i.e., time and cost), traffic delays, loss of business productivity and service interruption. In the United Kingdom (UK), about 60,000 utility strikes were documented each year, resulting in an estimated loss of 2.4 billion GBP annually (NUAR, 2021). There is a need to improve underground data quality and capture utility information in 3D. Surveying standards were established by regulatory authorities to ensure locational information of utilities were captured within sufficient confidence level. The required confidence level (horizontally and vertically) of surveyed as-built utilities are $\pm 250\text{mm}$, $\pm 100\text{mm}$ and $\pm 50\text{mm}$ in Denmark, Singapore, and the UK respectively (BSI, 2022; KEFM, 2019; SLA, 2021).

2. LITERATURE REVIEW

Recent innovations in Reality Capture technologies (laser scanners and photogrammetry techniques) have enabled the generation of visual-realistic 3D point clouds (PC) of objects and

their environments. Compared to photogrammetry, however, Terrestrial laser scanners (TLS) can be costly, not easily portable, and requires a steady platform to be set up on for data capture. To ensure full coverage, adjacent scanning sessions around an excavated trench would be required. However, the presence of heavy machinery, piles of construction materials and unstable ground conditions poses significant challenges. In this regard, photogrammetry offers flexibility in acquiring overlapping images from different angles around the pit, timeliness in data capture, and can be comparatively inexpensive, especially with the use of consumer-grade cameras (van Son et al., 2018). The rapid technological improvements in the fidelity of consumer-grade cameras and cloud storage over the last decade offer new opportunities for mainstream mobile photography and lost-cost sensor image acquisition, thereby facilitating the democratisation of photogrammetry for 3D surveys.

2.1 Consumer-grade Cameras for Photogrammetry

Extensive research efforts have been undertaken to understand the accuracy issues associated with consumer-grade cameras. Various camera-related factors, such as resolution, approximated principal distance, and lens distortion (radial and decentering distortions) affects measurement accuracy (Dai et al., 2014). Errors associated with lens distortion can usually be accounted for using mathematical models (Brown, 1971). Similarly, the work of González-Jorge (2011) echoed the importance of proper camera calibration and having good quality camera models for accurate and precise photogrammetry measurement tasks.

Akca and Gruen (2009) evaluated the geometric and radiometric performances between mobile phone and digital cameras. It was concluded that mobile phones are suitable for photogrammetry applications as the worst result (Sony Ericsson K750i) still offers millimetre level accuracy. Jaud et al. (2019) also evaluated smartphones and digital cameras using the Structure-from-Motion (SfM) technique for geomorphological reconstruction. By comparing the cloud distances between the cameras' PCs and a TLS dataset, results showed that centimetre level accuracy was

achieved regardless of the smartphone models used. These research highlights the maturity of employing consumer-grade cameras for data capture and 3D reconstruction.

2.2 Photogrammetry for Subsurface Utility Mapping

Many of the existing photogrammetric applications are applied to the 3D reconstruction of objects situated above a surface, leaving a gap in understanding the photogrammetric potential for mapping excavated trenches. A commendable study by Hansen et al. (2021) assessed the locational accuracy of water utilities by comparing two approaches: SfM technique with total station and GNSS-RTK. Smartphone-based video recordings of excavated pits were recorded, and it was concluded that the photogrammetric technique was a useful surveying method for capturing as-built utilities. However, while debatable, the accuracy of the reconstruction could potentially be affected by the less-than-ideal resolution of the images as they were extracted from a smartphone-based video recording. Therefore, the results remained contentious and warranted further investigation before a conclusion could be made about the reliability and the extensive use of smartphone cameras for utility surveys.

The study also highlighted several advantages of the photogrammetric solution. These include achieving time savings as the trench can be backfilled without needing to wait for registered surveyors to survey the exposed utilities, granted that proper Ground Control Points (GCPs) were marked around the pit. Generated PCs can be shared with asset owners for the planning of future utility projects, visualised using AR to avoid utility strikes (Hansen et al., 2020), serve as a quality assurance to clients and prove that nearby utilities were not damaged during excavation. Indeed, the use of smartphones-based images have great practicality for field engineers to acquire as-built information quickly and improve operational efficiency on construction sites. Moreover, PCs provide rich information (depth, dimensions, and component type), facilitating the ease of reconstructing structured 3D models and improving data quality.

However, to encourage confident adoption of photogrammetric technique as an accurate and reliable surveying approach, field engineers need to recognise how different image acquisition protocols affect the accuracy of utility mapping and to better plan their measurement routines. These protocols replicate realistic conditions a field engineer would likely encounter on site. For instance, should an engineer be pressed for time, what would be the minimum number of images required for a sufficient accurate measurement?

Multiple studies on how different imaging settings affect photogrammetric surveys have been conducted in other fields of applications, but not for underground mapping. Dai et al. (2014) highlighted how factors such as the amount of image overlaps, number of photos, camera intersection angles, shooting distances and baselines play a role in affecting accurate 3D reconstruction. A poor imaging network can undermine the estimation of interior camera parameters due to the instabilities within the least-squares bundle adjustment (Fraser, 1982). A strong network needs to have a sufficient number of intersecting rays on the object and good convergence angles (Remondino & Fraser, 2005). Similarly, some authors explored how the use of oblique and nadir photos influences the precision and accuracy of photogrammetric measurements. For example, Amrullah et al. (2016) and Bi et al. (2021), concluded that measurements do improve with the combination of oblique and nadir images during an aerial survey.

The continuous reduction in the cost of consumer-grade cameras and ease of utilising image processing pipelines hence present new opportunities for the application of photogrammetry for underground asset mapping. This paper first examines the potential of consumer-grade cameras for accurate subsurface utility surveys using SfM photogrammetry. Two different grades of smartphones, Samsung S20 Ultra and Motorola XT1092, and a digital camera, Nikon D3200, were used. Two metrics were employed to quantify the potential of the cameras. First, the Cloud-to-Cloud (C2C) distance between a reference PC, captured using a TLS, and the SfM PCs was used to assess the capability of the cameras in the 3D geometric reconstruction of utilities. A smaller C2C distance would mean greater potential as the reconstructed SfM PCs are able to replicate the geometry of the utilities. Second, the locational accuracy metric, measured in terms of horizontal and vertical root mean square error (RMSE), was used to compare the location of the utilities in the reference PC and the SfM PCs. Lower RMSE value would mean greater potential of the cameras in mapping the location of the utilities. The second part of the paper examines different image capture protocols using the S20 smartphone. Using the locational accuracy metric, protocols that yield the lowest locational error were recommended as an easy-to-understand guidelines for image acquisition at trenches of underground assets.

3. METHODOLOGY

3.1 Fieldwork Site

Fieldwork was conducted on an excavated trench located at Lidlington Place, London, UK (Figure 1). A building is located north of the trench and a pile of cable ducts were beside it. The pit is approximately 2.5m by 2m wide, not deeper than 1.2m. Three telecommunications (approximate depth of 0.25m) and two electric cables (approximate depth of 0.6m) were surveyed. 11 GCPs were collected using GNSS-RTK (Figure 2 and 3) and the four GCPs with the best 3D coordinate quality (3D CQ) values were used for georeferencing. The WGS84 3D coordinates were transformed and projected into British National Grid (BNG) and Ordnance Datum Newlyn (ODN). Checkpoints (CPs) were also manually marked on the utilities before image capture, and they serve as a common reference point for comparing the coordinates of the utilities in the reference PC to the coordinates of the corresponding utilities in the SfM PC.

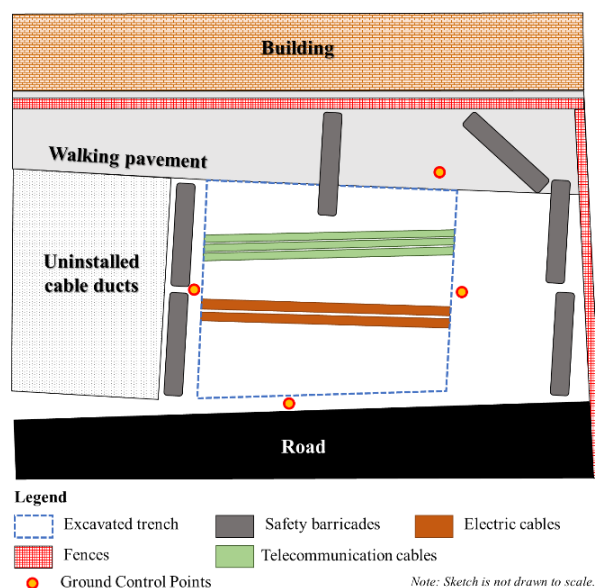


Figure 1. Site sketch of excavated trench and GCPs.

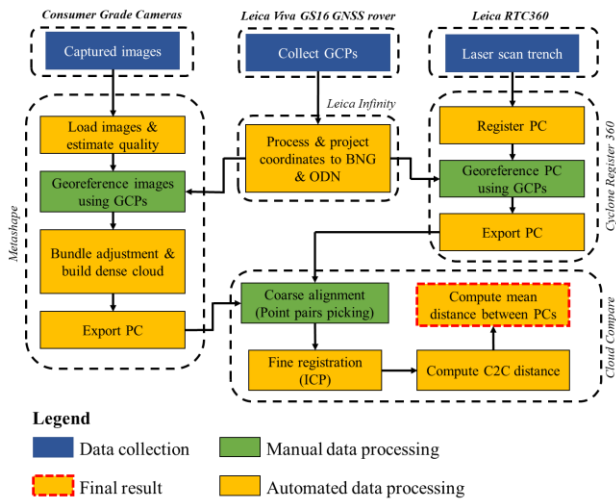


Figure 2. Workflow for computing cloud-to-cloud distance.

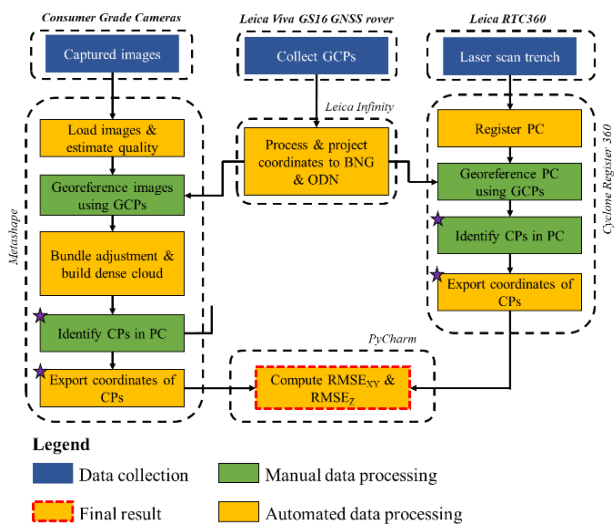


Figure 3. Workflow for computing locational accuracy.

3.2 Computing Cloud-to-Cloud Distance

Captured images from the S20, XT1092 and D3200 were loaded into *Metashape* (Agisoft, 2022) for 3D reconstruction (Figure 2). All images were then georeferenced by inserting markers within the captured image material. Following which, the bundle adjustment and the dense 3D reconstruction were performed before the SfM PCs were exported for comparison with the reference PC in *Cloud Compare* (CloudCompare Development Team, 2022). The reference PC serve as ground truth for all comparative measurements with the SfM PCs. To ensure a reliable reference dataset, a survey grade TLS, the *Leica RTC360 3D Laser Scanner*, was employed. A coarse alignment between the SfM and reference PCs was then executed by picking four pairs of points that corresponds to the location of the GCPs. Subsequently, a fine registration using the Iterative Closest Point (ICP) algorithm was performed. The closest-point distance method was used to compute the mean C2C distance due to its statistical simplicity. As compared to the commonly used multi-scale model to model cloud comparison (M3C2) approach, it would be very challenging to determine suitable statistical

parameters especially with limited knowledge of the characteristics of the PCs to be analysed (Lague et al., 2013).

3.3 Computing Locational Accuracy

The workflow used to compute the locational accuracy metric is largely similar to the C2C metric, except the only difference was identifying the coordinates of 16 CPs in both the SfM and reference PCs in their respective software and extracting them for comparison (differences are marked in purple stars in Figure 3). The horizontal ($RMSE_{xy}$) and vertical ($RMSE_z$) error measurements of the SfM and reference PCs were computed in accordance with the Geospatial Positioning Accuracy Standard (FGDC, 1998). A script was developed to automate the calculation of RMSE values for the different cameras and image capture protocols.

3.4 Image Capture Protocols

Three rounds of testing were performed to isolate the effects of multiple changing protocols on the RMSE values. These protocols include stand-off distance to trench, geometry of image network, availability of nadir images, number of images captured, and orientation of images to utilities. In each round, individual sequences have their protocols varied (Appendix A). For example, in sequences 2 and 4, the only varying protocol is the stand-off distance. The sequence that performs the best from the previous round will have their protocols further varied in the subsequent round.

A total of 21 sequences were tested. Sequences 1 to 8 were tested in round 1. There were two stand-off distances, at 0.5m and 1.0m away from the boundary of the trench. For each distance, images were collected using two different geometry networks, ‘linear-shaped’ and ‘fan-shaped’ (Figure 4). In the linear approach, one photo was taken at each viewpoint located along the same distance from the pit. In the fan-shaped approach, five divergent photos were taken from each viewpoint along the same distance from the pit. A selfie stick was used to capture nadir images. Sequences 9 to 17 were performed in round 2. The number of photos was reduced systematically by having one viewpoint (consisting of five divergent photos) removed sequentially from the extreme left of each side of the trench. Images were reduced in this manner to allow the camera network to maintain sufficient overlapping photos, where parts of the trench that were missing images will remain visible from the set captured on the corresponding opposite side. Partial and complete removal of nadir photos were also tested. In round 3, sequences 18 to 21 were performed. Images (camera rays) that were perpendicular and parallel to the direction of the utilities were evaluated, followed by the complete removal of nadir photos.

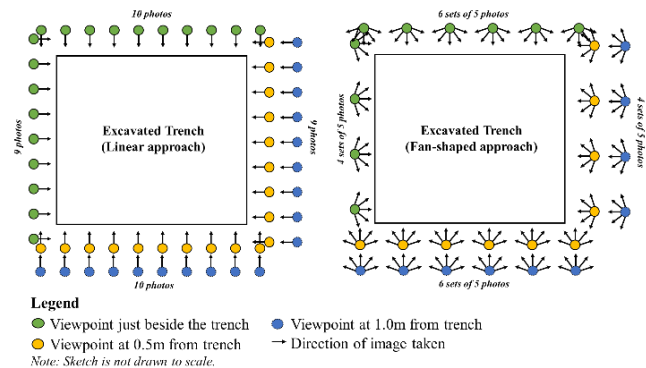


Figure 4. Geometry of image network.

4. RESULTS AND DISCUSSION

4.1 Assessing the Potential of Consumer-grade Cameras

This section presents the results of both metrics that were employed to quantify the potential of consumer-grade cameras.

4.1.1 Cloud-to-Cloud Distance

The XT1092, S20 and D3200 have a mean distance of 14.4mm, 27.6mm, 18.2mm, and a standard deviation of 13.3mm, 35.9mm and 18.5mm respectively (Figure 5). Theoretically, it was expected that the D3200 perform the best because of its superior technical specifications. The work of Jaud et al. (2019) also demonstrated that PCs reconstructed from digital cameras have lower C2C distances than smartphone PCs. However, this was not the case.

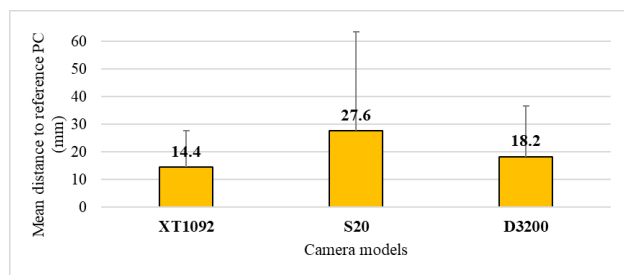


Figure 5. C2C distances between SfM and reference PCs.

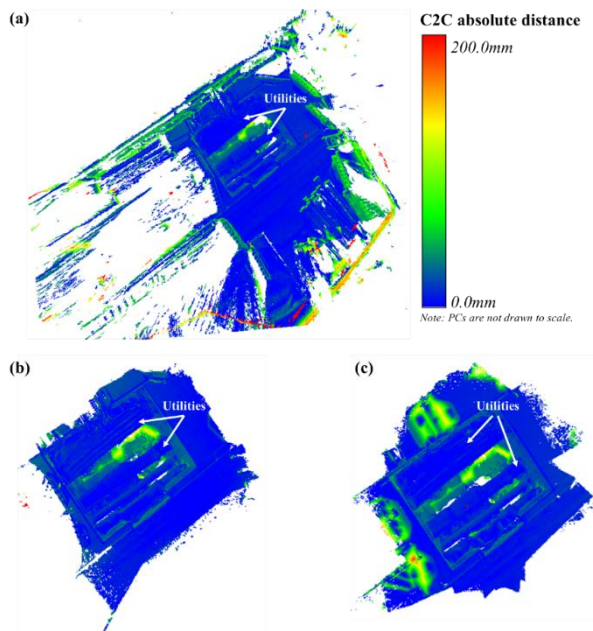


Figure 6. C2C distance for (a) S20, (b) XT1092 and (c) D3200.

Figure 6 reveals that the S20 PC had a high number of points with large distance variations located in areas near the fences and safety barricades, accounting for its large standard deviation. The D3200 experienced relatively less distance variation (mainly concentrated at the safety barricades located beside the trench) while the XT1092 had the lowest variation. These observations clearly explain the results in Figure 5 where the C2C distances were averaged from values with large distance variations, therefore resulting in the poor performance of the S20, and the D3200 performing worse than the XT1092. Although the differences in the mean PC density of the cameras could affect

the computation of the point-to-point distances in both the SfM and reference PC (Lague et al., 2013), the magnitude of the differences in the C2C distance between the SfM PCs were rather minimal (range is ~13mm apart). In addition, it was observed that the C2C distances of the pipes in all the SfM PCs were within the blue-coloured range (~0.0mm), suggesting that all cameras were successful in replicating the geometry of the utilities.

4.1.2 Locational Accuracy

The D3200 performed best with a horizontal and vertical RMSE value of 34.7mm and 11.9mm respectively (Figure 7). Both smartphones performed similarly in terms of their horizontal error at 35.1mm. However, the S20 had a higher vertical RMSE at 12.8mm as compared to the XT1092 at 12.2mm.

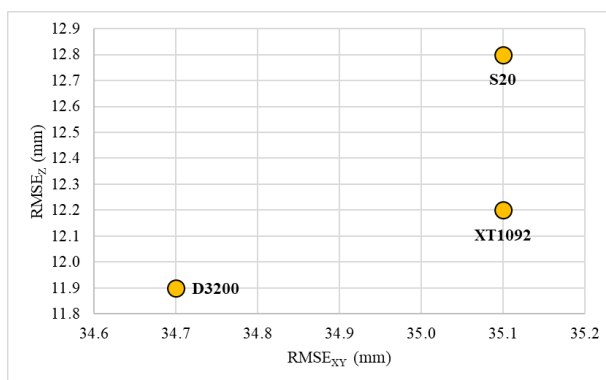


Figure 7. Horizontal and vertical errors across camera models.

These findings are in alignment with existing literature in observing that digital cameras outperform mobile phone cameras due to their better camera quality (Akca & Gruen, 2009). The results of the smartphones' horizontal errors were largely similar to the results in Hansen et al. (2021) where a RMSE_{XY} of 30.4mm was achieved. However, the vertical errors differed by around 20mm (the authors reported a RMSE_Z of 32.6mm). These differences could likely be attributed to the following reasons. First, poor precision is often related to vertical GNSS measurements (Irughe & Audu, 2016) and the likely less-than-ideal image resolution from smartphone-captured videos could have affected the bundle adjustment process. Second, the use of the RMSE indicator could have inflated the RMSE_Z value due to the heavy penalisation of outliers during its calculation.

Differences in the locational errors of the cameras could be explained by two possible reasons. First, the differences in the ground sampling distance (GSD) values across the cameras play a role in introducing potential inaccuracies during the geo-referencing process (Table 1).

Camera models	GSD (mm/pix)	Reprojection error (pix)	Normalised reprojection error (mm)
XT1092	0.6	1.06	±0.7
S20	1.2	0.77	±1.0
D3200	0.4	0.99	±0.3

Table 1. Photogrammetric parameters of SfM PCs.

A camera with a high GSD value would have lower spatial resolution and lesser ability to capture fine details in the photos. As such, a marker not placed on the exact pixel containing the GCPs (even if just one pixel away from the original GCP position) would introduce an error equivalent to the product of

the GSD value and the number of misaligned pixels during the georeferencing process. In the case of the worst performing S20, the relatively high GSD value would mean the possibility of introducing a 1.2mm blunder as compared to making a 0.4mm and 0.6mm error with the D3200 and XT1092 respectively. GSD values can also be influenced by the type of camera lens. A pronounced lens curvature (the S20 has an ultra-wide-angle lens) would result in an increase in the GSD value of the pixels at the edge of the image relative to the pixels located in the centre of the image (Booth et al., 2006). Hence, it would be preferable to avoid using wide-angle lenses for photogrammetric utility surveying as they have the potential to introduce more errors. The superior quality of the digital camera over smartphone cameras is therefore evident in the former's lower GSD value.

Second, the differences in the cameras' locational errors could be attributed to the ability to correct for camera distortions and the quality of the bundle adjustment in 3D space. An examination of the residual patterns of the cameras reveals the inability of the Brown's model (Brown, 1971) in accounting for lens distortion in smartphone cameras (Figure 8).

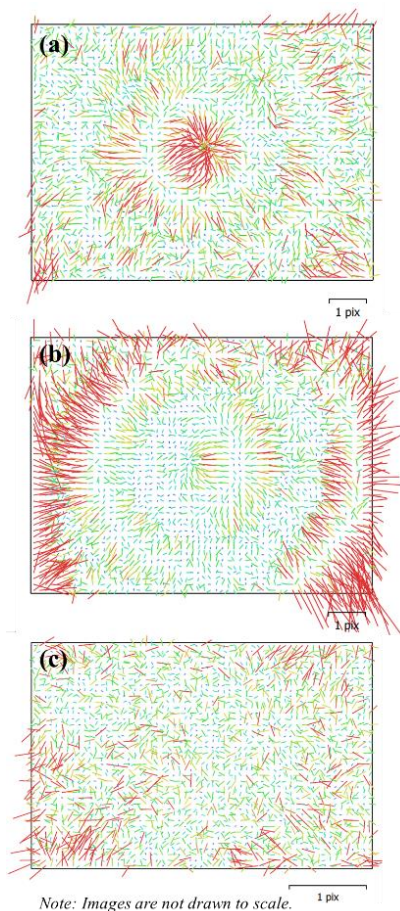


Figure 8. Image residuals of (a) XT1092, (b) S20 and (c) D3200 after bundle adjustment.

Systematic errors were observed in the smartphones' photos, with a high number of residuals found in the centre of the XT1092 and at the edges of the S20 image. Conversely, the lower number of residuals in the D3200 are more chaotically spread out, exhibiting a random pattern across the image, suggesting better performing self-calibration during the bundle adjustment process. This deduction is further supported by the lowest normalised reprojection error (NRE) value of the D3200 where

the internal precision of the bundle adjustment was $\pm 0.3\text{mm}$. The NRE was calculated using the product of the GSD value and the reprojection error (Table 1), allowing a fair comparison of the internal precision of the bundle adjustment of the cameras in absolute ground units (mm). As compared to the higher image residuals and NRE values of the XT1092 ($\pm 0.7\text{mm}$) and S20 ($\pm 1.0\text{mm}$), it was without surprise that the performances of the bundle adjustment of the smartphones were less precise, therefore resulting in higher locational errors. The image residuals and the achieved locational accuracy results underscore the work of González-Jorge (2011) which emphasised the importance of proper camera calibration for accurate and precise photogrammetry measurement tasks.

An interesting observation was the S20, a considerably higher-grade smartphone than the XT1092, performing the worst. This could likely be attributed to the S20's camera characteristics (ultra-wide-angle lens and lower resolution at 12MP). As such, to attain accurate and precise surveys, one should always aim for a higher resolution camera (Dai et al., 2014) and avoid the use of wide-angle lenses. Nevertheless, the RMSE results were not surprising as the D3200 had better lens quality as compared to smartphone cameras.

4.2 Minimising Locational Errors with Best Photogrammetric Data Capture Practices

This section presents the results from the different image capture protocols. In the first round, sequence 8 performed the best with a horizontal and vertical error of 34.7mm and 12.4mm respectively (Figure 9). As compared to the linear-shaped geometry (sequences 1, 3, 5, 7), it was observed that the fan-shaped geometry (sequences 2, 4, 6, 8) generally performed better with lower vertical errors, except for sequences 2 and 4 which have relatively higher horizontal errors than sequences 3 and 7 by a maximum of 0.2mm. This outcome agrees with existing literature (Remondino & Fraser, 2005; Wackrow & Chandler, 2011), where the presence of convergent images minimises photogrammetric errors. In a fan-shaped geometry network, the chances of having intersecting camera rays that are close to the 90° angle between the different divergent photos from each viewpoint and its neighbouring set of images are much higher than in the linear-shaped approach.

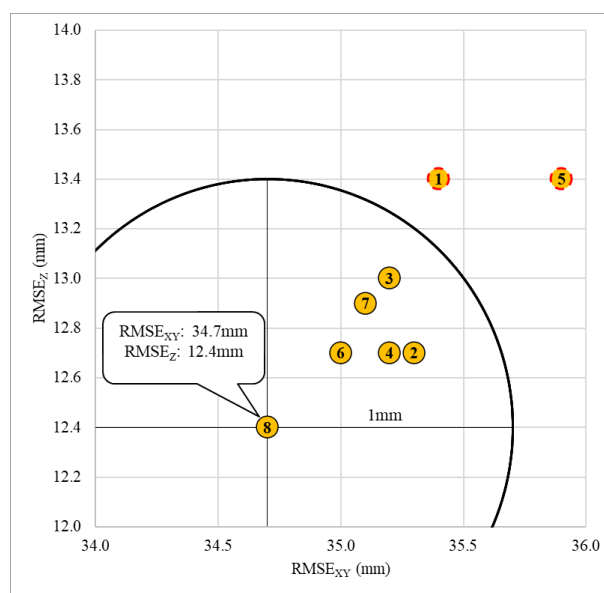


Figure 9. Results from first round of testing.

In the case of stand-off distances, existing works have shown how an increase in distance from the object of interest can lead to greater errors (Dai & Lu, 2013) and a greater number of overlapping images (Jaud et al., 2019). Although sequence 8 performed the best, the achieved results are rather inconclusive as the errors of the other 7 sequences vary almost randomly with no identifiable pattern. This might be due to the limitations of the site conditions where the shooting distance could not be varied on two sides of the trench (the presence of the building and uninstalled cable ducts). Nevertheless, regardless of the shooting distance, all 8 sequences achieved sufficient overlapping images. As such, it would be reasonable to conclude that, in this case, having a distance variation of 0.5m between viewpoints might not have a great impact on the accuracy as there was sufficient image redundancy. It was also observed that sequences 6, 7 and 8 achieved lower horizontal errors than sequences without nadir photos. The availability of nadir photos might have helped tighten the self-calibration process by providing greater visibility of the utilities and surrounding environment due to its plan view perspective. This result draws similarity to existing works where a combination of nadir and oblique aerial images improved the measurement results (Amrullah et al., 2016; Bi et al., 2021).

The NRE value of the S20 revealed that the internal precision of the bundle adjustment process was within $\pm 1.0\text{mm}$. Therefore, sequences that scored within the circle (1mm radius drawn to scale in Figure 9) would be deemed acceptable as the variations in their errors were within the range of the noise measurements. As a result, sequences 1 and 5 were considered outliers. However, their error values were within sub-mm deviation from the boundary of the circle, and this was likely due to errors associated with human vision and dexterity in marking the CPs in the SfM PC. Given the inconsequential differences, the image capture protocols of sequences 1 and 5 are also considered acceptable for field engineers' adoption, but not recommended given its linear-shaped geometry network.

In the second round (Figure 10), all sequences were captured at 1.0m away from the trench using the fan-shaped geometry approach. Sequence 11 and 12 (consisting of 52 and 42 photos respectively, with nadir images) performed best with a horizontal error of 34.3mm and 34.2mm, and a vertical error of 12.3mm and 12.7mm respectively.

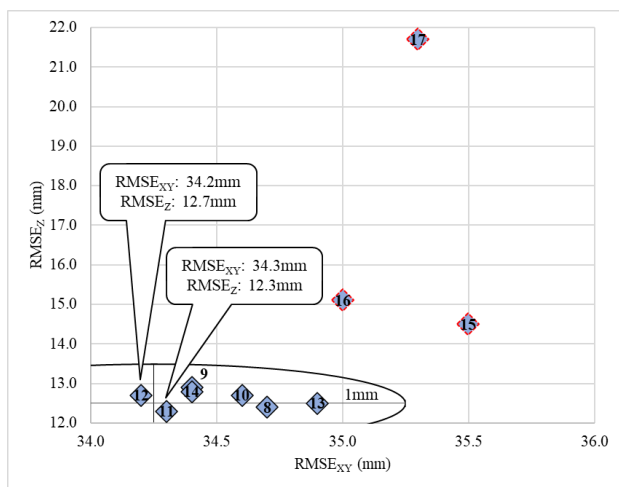


Figure 10. Results from second round of testing.

Likewise, sequences that are within the 1mm precision are considered acceptable and they have images varied from 26 to

112 photos with the inclusion of nadir photos. Sequences 15, 16 and 17 were the worst performing where nadir images were not included, and they all had fewer than 21 images. The errors increased significantly when the number of images dropped to 8 photos (sequence 17), especially in the vertical dimension. In situations where engineers are unable to capture nadir images on site, a minimum of 38 images (sequence 2, 3 and 4) should be captured to avoid undesirable measurements. If nadir images are available, a minimum of 26 images would be ideal for mapping the location of the utilities within reasonable accuracy.

In the third round (Figure 11), 52 photos were used for processing in all sequences. Sequence 18 (camera rays orientated perpendicular to utilities with nadir photos) had the lowest RMSE_{XY} (34.0mm) and RMSE_Z (12.1mm) values. Conversely, sequence 20 (nadir photos were also available) performed worse when the camera rays were parallel to the utilities. This was likely due to the inability of the camera rays in capturing sufficient details of the pipes for proper 3D reconstruction. Comparing between sequences 19 and 21 (where nadir photos were not available in both), the perpendicular approach still performed better than the parallel approach. This goes to show the importance of maximising the visibility of the object required for surveying (Galantucci et al., 2006). Even with the use of both parallel and perpendicularly shot images helped improve overall image coverage of the object of interest (see Figure 12 where sequence 11 and 18 did better than sequence 20). Nonetheless, a similar trend was again observed, where the lack of nadir images (sequences 19 and 21) resulted in higher error values.

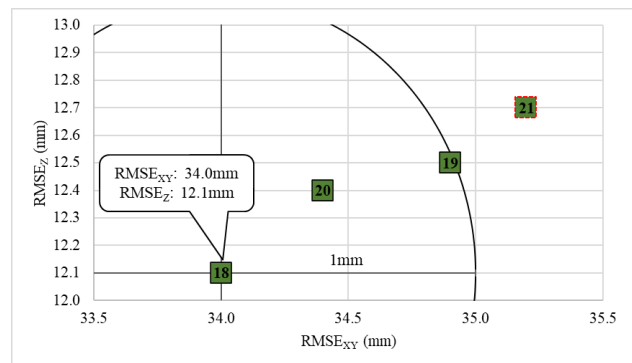


Figure 11. Results from third round of testing.

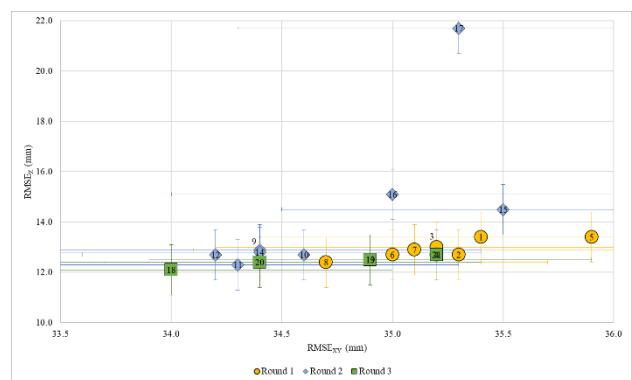


Figure 12. Horizontal and vertical errors for sequences 1 to 21.

The variability of the errors in all the sequences (except 15, 16 and 17 in Figure 12) differed by 2mm horizontally (34mm to 36mm) and vertically (12mm to 14mm). These sequences all had overlapping error bars suggesting that the errors were very

similar to each other regardless of the image capture protocols tested. The variability in these sequences could be attributed to human errors during the georeferencing and CPs identification process, and the background noise within the S20. On the other hand, the error bars of sequences 15, 16 and 17 deviated from the rest, suggesting the significant influence of particular image capture protocol(s) being adopted. These three sequences shared similar protocol characteristics: having a low number of photos (20 photos and below) and the non-availability of nadir images.

Based on the results, the following best photogrammetric practices are recommended for field engineers. First, engineers should aim to capture photos using the fan-shaped approach to maximise the angle of intersection between camera rays. Even when obstacles hinder the engineer from continuously capturing a full round of images around the trench, snapping multiple divergent images from different viewpoints around the pit is acceptable granted a minimum number of photos were used. Second, a minimum of 38 images should be acquired when nadir images are not available. If pressed for time, engineers should still aim for a minimum of 26 images, but nadir photos must be acquired. Given the low cost of capturing photos and the portability of using a selfie stick, capturing nadir images will always be encouraged. Third, engineers should always aim to maximise object visibility and avoid taking photos where the camera rays are parallel to the utilities' orientation. Finally, photos should be captured within 1.0m from the trench.

4.3 Consumer-grade Cameras as a Photogrammetric Utility Data Acquisition Tool

The achieved locational accuracies of the XT1092, D3200, and the RMSE values of all 21 sequences (derived from the S20) were observed to be within the confidence levels of the surveying standards established by Denmark, Singapore and the UK. All cameras were also successful in the 3D geometric reconstruction of the utilities. The minimal differences in the C2C distances of the cameras demonstrated that smartphones performed almost on par with the digital camera. These findings suggested the reliability and suitability of using consumer-grade cameras, especially smartphones, as a photogrammetric data acquisition tool for subsurface utility surveys. Nevertheless, the ability to collect accurate and reliable data is still limited by the availability of low 3D CQ GNSS values for accurate georeferencing. Commercial solutions like the viDoc RTK become attractive to engineers as they promise absolute centimetre-level accuracy (PIX4D, 2022), removing the need for heavyweight GNSS rovers to conduct GCP measurements. However, further assessment of such solutions would be needed, especially in situations where multipath and Non-Line-of-Sight effects are strong, before the true potential of using smartphones for utility surveying can be maximised.

The next step is to drive the adoption of consumer-grade cameras for utility survey. This can be achieved by setting up a Community of Practice, engaging different parties involved in the underground mapping ecosystem, building awareness, and exchanging knowledge on best practices for photogrammetric surveys. An example is the Digital Underground Connect initiative in Singapore, where workshops and demonstrations were held bimonthly to discuss issues related to underground utility mapping (Singapore-ETH Centre et al., 2022). Government authorities can potentially set aside innovation funds to help utility asset owners implement photogrammetric surveying into their operations, and then rolling out policies that advocate the submission of 3D utility data models. Commercialised solutions like PIX4D, hence play an important

role as technological innovators in streamlining and automating the use of smartphone cameras for accurate and reliable photogrammetric surveys. It is important to have the public and private sector collaborate, adopting relevant policy and technology to bring greater economic and social benefits for society and individuals.

5. CONCLUSION

In conclusion, this paper addresses the issue of poor documentation of utility data and aim to improve operational efficiency on construction sites by investigating the use of consumer-grade cameras and different imaging settings for photogrammetric low-cost subsurface utility surveys. Results from the first part of the study demonstrated the fidelity of smartphone cameras in the 3D reconstruction of subsurface utilities, and its great potential as a photogrammetric utility data acquisition tool. However, the statistical insights from the photogrammetric calibration show that caution needs to be taken about the camera types particularly for lens calibration. In the second part, results demonstrated the need for field engineers to (i) capture multiple divergent photos from each camera location surrounding the trench, (ii) acquire a minimum of 26 images when nadir images are available, else, a minimum of 38 images, (iii) maximise object visibility, and (iv), capture photos within 1.0m from the trench. Although further studies on different trenches would be required to generalise these results, the findings of this paper could be extended to other terrestrial close-range smartphone based SfM projects.

Over time, with increasing adoption of photogrammetry as a utility mapping technique, a repository of visual-realistic subsurface information will benefit the parties involved in the underground infrastructure ecosystem. Planners and excavators will be equipped with accurate and reliable information for effective planning, construction, and maintenance work of underground services, thereby improving operational efficiency on construction sites, reducing the risks of utility strikes and disruptions to citizens.

ACKNOWLEDGEMENTS

The authors would like to thank the United Kingdom's Geospatial Commission (National Underground Asset Register) and the Singapore Land Authority in support of this project. Special thanks to Skanska UK and SCS Railways for providing an excavated site to conduct the experiments, and the staff and students of UCL for their assistance rendered during fieldwork.

REFERENCES

- Agisoft. (2022). *Metashape Software* (Professional Edition version 1.8.3 (64 bit)). Agisoft LLC. <https://www.agisoft.com/>
- Akca, D., & Gruen, A. (2009). Comparative Geometric and Radiometric Evaluation of Mobile Phone and Still Video Cameras. *The Photogrammetric Record*, 24(127), 217–245.
- Amrullah, C., Suwardhi, D., & Meilano, I. (2016). Product Accuracy Effect of Oblique and Vertical Non-metric Digital Camera Utilization in UAV-Photogrammetry to Determine Fault Plane. *ISPRS Annals of Photogrammetry, Remote Sensing and Spatial Information Sciences*, III–6, 41–48. <https://doi.org/10.5194/isprsannals-iii-6-41-2016>
- Bi, R., Gan, S., Yuan, X., Li, R., Gao, S., Luo, W., & Hu, L. (2021). Studies on Three-Dimensional (3D) Accuracy Optimization and Repeatability of UAV in Complex Pit

- Rim Landforms As Assisted by Oblique Imaging and RTK Positioning. *Sensors*, 21(23). <https://doi.org/10.3390/s21238109>
- Booth, D. T., Cox, S. E., & Berryman, R. D. (2006). Precision measurements from very-large scale aerial digital imagery. *Environmental Monitoring and Assessment*, 112(1–3), 293–307. <https://doi.org/10.1007/s10661-006-1070-0>
- Brown, D. C. (1971). Close-Range Camera Calibration. *Photogrammetric Engineering*, 855–866.
- BSI. (2022). *PAS 128: 2022*.
- CloudCompare Development Team. (2022). *CloudCompare* (2.0). Open Source Project. <https://www.danielgm.net/cc/>
- Dai, F., Feng, Y., & Hough, R. (2014). Photogrammetric error sources and impacts on modelling and surveying in construction engineering applications. *Visualisation in Engineering*, 2(2).
- Dai, F., & Lu, M. (2013). Three-Dimensional Modeling of Site Elements by Analytically Processing Image Data Contained in Site Photos [Article]. *Journal of Construction Engineering and Management*, 139(7), 881–894. [https://doi.org/10.1061/\(ASCE\)CO.1943-7862.0000655](https://doi.org/10.1061/(ASCE)CO.1943-7862.0000655)
- FGDC. (1998). *Geospatial Positioning Accuracy Standards Part 3: National Standard for Spatial Data Accuracy*.
- Fraser, C. S. (1982). On the use of nonmetric cameras in analytical close-range photogrammetry. *Canadian Surveyor*, 36(3), 259–279. <https://doi.org/10.1139/TCS-1982-0030>
- Galantucci, L. M., Percoco, G., & Ferrandes, R. (2006). Accuracy Issues of Digital Photogrammetry for 3D Digitization of Industrial Products. In *Revue Internationale de Ingegnerie Numerique* (Vol. 2). <https://www.researchgate.net/publication/225308166>
- González-Jorge, H. (2011). Verification artifact for photogrammetric measurement systems. *Optical Engineering*, 50(7), 073603. <https://doi.org/10.1117/1.3598868>
- Hansen, L. H., Pedersen, T. M., Kjems, E., & Wyke, S. (2021). Smartphone-based Reality Capture for Subsurface Utilities: Experiences from Water Utility Companies in Denmark. *International Archives of the Photogrammetry, Remote Sensing and Spatial Information Sciences - ISPRS Archives*, 46(4/W4-2021), 25–31. <https://doi.org/10.5194/isprs-archives-XLVI-4-W4-2021-25-2021>
- Hansen, L. H., Wyke, S. S., & Kjems, E. (2020). *Combining Reality Capture and Augmented Reality to Visualise Subsurface Utilities in the Field*. 2020, 703–710.
- Irughe, R. E., & Audu, A. P. (2016). Determination of Horizontal and Vertical Positional Accuracy from GNSS Geodetic Observations. *Tropical Environment*, 13(1), 34–45. <https://www.researchgate.net/publication/311681615>
- Jaud, M., Kervot, M., Delacourt, C., & Bertin, S. (2019). Potential of Smartphone SfM Photogrammetry to Measure Coastal Morphodynamics. *Remote Sensing*, 11(2242).
- KEFM. (2019). *LER-bekendtgørelsen*. Ministry of Climate, Energy and Supply. <https://www.retsinformation.dk/eli/ta/2019/1473?id89f3d05a-86b1-4773-bbdc-1a01c55b0f1b>
- Lague, D., Brodu, N., & Leroux, J. (2013). Accurate 3D comparison of complex topography with terrestrial laser scanner: Application to the Rangitikei canyon (N-Z). *ISPRS Journal of Photogrammetry and Remote Sensing*, 82, 10–26. <https://doi.org/10.1016/j.isprsjprs.2013.04.009>
- PIX4D. (2022). *viDoc RTK Rover: The future of single point measurement with 3D scanning | Pix4D*. <https://www.pix4d.com/product/vidoc-rtk-rover>
- Remondino, F., & Fraser, C. (2005). Digital camera calibration methods: Considerations and comparisons. *ISPRS Commission V Symposium "Image Engineering and Vision Metrology,"* 266–272. <https://www.researchgate.net/publication/228672107>
- Singapore-ETH Centre, Singapore Land Authority, Bentley Institute Digital Advancement Academies, & Singapore Institute of Surveyors and Valuers. (2022). *Digital Underground Connect*. <https://www.duconnect.org/>
- SLA. (2021). *Standard and Specifications for Utility Survey in Singapore Version 1.1*.
- van Son, R., Jaw, S. W., Yan, J., Khoo, H. S. V., Loo, W. K. R., Teo, S. N. S., & Schrotter, G. (2018). A framework for reliable three-dimensional underground utility mapping for urban planning. *International Archives of the Photogrammetry, Remote Sensing and Spatial Information Sciences - ISPRS Archives*, 42(4/W10), 209–214. <https://doi.org/10.5194/isprs-archives-XLII-4-W10-209-2018>
- Wackrow, R., & Chandler, J. H. (2011). Minimising systematic error surfaces in digital elevation models using oblique convergent imagery. *Photogrammetric Record*, 26(133), 16–31. <https://doi.org/10.1111/j.1477-9730.2011.00623.x>

APPENDIX

Sequence	Stand-off distance to trench	Geometry of image network	Availability of nadir images	Number of images captured	Orientation to utilities
1	0.5m	Linear	No	38	Mix
2	0.5m	Fan	No	100	Mix
3	1.0m	Linear	No	38	Mix
4	1.0m	Fan	No	100	Mix
5	0.5m	Linear	Yes	50	Mix
6	0.5m	Fan	Yes	112	Mix
7	1.0m	Linear	Yes	50	Mix
8	1.0m	Fan	Yes	112	Mix
9	1.0m	Fan	Yes	92	Mix
10	1.0m	Fan	Yes	72	Mix
11	1.0m	Fan	Yes	52	Mix
12	1.0m	Fan	Yes	42	Mix
13	1.0m	Fan	Yes	32	Mix
14	1.0m	Fan	Yes	26	Mix
15	1.0m	Fan	No	20	Mix
16	1.0m	Fan	No	12	Mix
17	1.0m	Fan	No	8	Mix
18	1.0m	Fan	Yes	52	Perpendicular
19	1.0m	Fan	No	52	Perpendicular
20	1.0m	Fan	Yes	52	Parallel
21	1.0m	Fan	No	52	Parallel